Research article **Open Access**

Ruxue Li, Zhipeng Wei*, Fenghuan Zhao, Xian Gao, Xuan Fang, Yongfeng Li, Xinwei Wang, Jilong Tang, Dan Fang, Haizhu Wang, Rui Chen* and Xiaohua Wang

Investigation of localized and delocalized excitons in ZnO/ZnS core-shell heterostructured nanowires

DOI 10.1515/nanoph-2016-0157
Received September 2, 2016; revised October 27, 2016; accepted November 12, 2016

Abstract: The localized states in ZnO nanowires (NWs) through the growth of ZnS shell have been introduced in this paper. Morphology and optical properties of the ZnO/ZnS core-shell heterostructured NWs after different rapid thermal annealing (RTA) treatments are investigated. Transmission electron microscopy measurements show the gradual disappearing of the jagged boundary between ZnO and ZnS with the increase of RTA temperature, while a decrease of interfacial composition fluctuation and a formation of ZnOS phase can be found after a RTA treatment of 300°C. Temperature-dependent photoluminescence exhibits the features of "S-shape" peak positions and a "valley shape" for the emission width, implying the existence of localized excitons in the core-shell NWs. Moreover, it is noted that the RTA treatments can lower the localized degree which is confirmed by optical measurement. The results indicate that the optical behavior of excitons in ZnO/ZnS core-shell heterostructured NWs can be manipulated by appropriate thermal treatments, which is very important for their practical device applications.

Keywords: excitons; core-shell heterostructured nanowires; rapid thermal annealing; laser spectroscopy.

***Corresponding authors: Zhipeng Wei,** State Key Laboratory of High Power Semiconductor Lasers, School of Science, Changchun University of Science and Technology, 7089 Wei-Xing Road, Changchun 130022, P. R. China, e-mail: zpweicust@126.com; and **Rui Chen,** Department of Electrical and Electronic Engineering, South University of Science and Technology of China, Shenzhen, Guangdong 518055, P. R. China, e-mail: chen.r@sustc.edu.cn
Ruxue Li, Xian Gao, Xuan Fang, Jilong Tang, Dan Fang, Haizhu Wang and Xiaohua Wang: State Key Laboratory of High Power Semiconductor Lasers, School of Science, Changchun University of Science and Technology, 7089 Wei-Xing Road, Changchun 130022, P. R. China
Fenghuan Zhao: Department of Electrical and Electronic Engineering, South University of Science and Technology of China, Shenzhen, Guangdong 518055, P. R. China
Yongfeng Li: Key Laboratory of Physics and Technology for Advanced Batteries (Ministry of Education), College of Physics, Jilin University, Changchun 130012, P. R. China
Xinwei Wang: State Key Laboratory of High Power Semiconductor Lasers, School of Materials Science and Engineering, 7089 Wei-Xing Road, Changchun 130022, P. R. China

1 Introduction

Free excitons can be easily trapped by the spatially localized potential fluctuations in a certain small area to become localized excitons in crystals or films [1]. The localized states can expand the electronic density of state (DOS) to form an exponential tail instead of the sharp conduction and valance band edges. Localized states can be found in the semiconductor quantum structures and has become one of the characteristics which have been demonstrated to be responsible for the high emission efficiency of a variety of semiconductor composites [2–4]. For example, in the case of dilute nitride semiconductors, the localized excitons always present a so-called "S-shape" peak position feature obtained from the temperature-dependent photoluminescence (TDPL) measurement and a "valley shape" of full width at half maximum (FWHM) [1, 5]. These typical features can be described by a quantitative model proposed by Li et al. [5] and are widely used to verify the existence of localized excitons. It has been confirmed that the localized effect can prevent the generated carriers from defusing to non-radioactive recombination centers, thus enhancing the emission and the response range of light. Therefore, at present, the localized states in the semiconductor nanomaterial have stimulated intensive research attention for high-performance excitonic optoelectronic devices, such as light-emitting diodes (LEDs), lasers, solar cells, and photodetectors [6–12].

The ZnO (E_g = 3.37 eV) semiconductors, which possess a large exciton binding energy of 60 meV, are widely used for ultraviolet (UV) photoelectric devices [13–19]. However, the room temperature emission from ZnO nanostructures always display a broad deep level emission (DLE) in the

visible region along with the weak near-band edge (NBE) emission in the UV region. These greatly affect the performance of ZnO materials, especially for nanostructures that have a large surface-to-volume ratio. To solve the problem, strategies of new nanocomposite structures or passivating the surface of ZnO (such as the surface coating of organic polymers or epitaxial growth of heterogeneous semiconductors) have been proposed and carried out [20–24]. Among them, one of the most effective ways is the core-shell heterostructures. Chen et al. have fabricated ZnO-based core-shell nanowire (NW) structure by the surface modification technique [7]. They found that the enhanced UV emission after high-energy argon ion (Ar^+) milling can be ascribed to the localized excitons from the ZnO-based core-shell NW structure. Recently, in our group, ZnO/ZnS core-shell NWs were successfully synthesized by wet chemical method, in which localized exciton phenomena were found after the ZnS growth on ZnO NWs. The ZnO/ZnS nanocomposite structures exhibit remarkable UV photoresponse and enhanced electroluminescence from LEDs, which have been ascribed to the existence of localized states in the material system [6, 8].

According to the previous reports, the localized states have a great impact on the optical properties of the nanomaterial. Therefore, how to introduce and regulate localized states has aroused widespread interest. To the best of our knowledge, there have been very few literature reports about controlling of localized excitonic behaviors, especially for ZnO core-shell nanostructures. Hence, it is highly desirable and significant, as well as a big challenge, to develop an effective and convenient method to manipulate the localized excitons and their corresponding properties. In this paper, through the growth of ZnO/ZnS core-shell heterostructured NWs, we have introduced localized states in the core-shell interface between the ZnO and ZnS. After subsequent thermal treatments, the optical properties of the localized excitons have been discussed based on laser spectroscopy [1–8]. The underlying physical mechanism of the change of localized excitons after thermal treatments has also been proposed and discussed in detail.

2 The experimental system

2.1 Materials synthesis

Zinc acetate dehydrate [$Zn(CH_3COO)_2{\cdot}2H_2O$], hexamethylenetetramine ($C_6H_{12}N_4$), sodium sulfide (Na_2S), and zinc nitrate hexahydrate [$Zn(NO_3)_2{\cdot}6H_2O$] were of analytical grade. All chemicals were supplied by Guangfu Chemical Reagent Factory in Tianjin, China, and the reaction device of teflon-lined a stainless steel autoclave was provided by YiChuang company from Xi'an, China. They were used without further purification. Synthesis of ZnO NWs: In our synthetic system, the ZnO seeds were deposited on sapphire substrate by atomic layer deposition. Subsequently, the nucleations of ZnO NWs were synthesized by typical solvothermal reactions. The detailed processes of synthesis are provided in our previous reports [6]. Synthesis of ZnO/ZnS core-shell heterostructured NWs: To prepare ZnO/ZnS core-shell heterostructured NWs, the as-grown ZnO NWs were immersed in 0.16 mol/l sodium sulfide (Na_2S) and zinc nitrate [$Zn(NO_3)_2$] solution for 2 h at 60°C. Finally, the samples of the ZnO/ZnS NWs were cleaned with deionized water and were dried under normal conditions.

2.2 Rapid thermal annealing

The synthesized ZnO/ZnS core-shell heterostructured NWs were annealed at 200, 250, and 300°C in a flowing N_2 gas ambient for 30 s. For easier reading, the corresponding samples after the treatments are indexed as RTA-200, RTA-250, and RTA-300, respectively.

2.3 Materials characterization

A Hitachi S-4800 field emission scanning electron microscope and X-ray diffraction (XRD) with a Bruker D8 advance X-ray powder diffractometer with Cu K_α radiation ($\lambda = 1.5406$ Å) were used to characterize the composition of the samples. The transmission electron microscopy (TEM) images were obtained using a FEI Tecnai G2 F20 microscope operated at 200 kV. Photoluminescence (PL) measurements were performed with a ZoLix Omni λ 500 spectrograph, and a conventional backscattering geometry was used to collect the emission. Moreover, the temperature of the samples was controlled between 10 and 300 K by a closed-cycle helium cryostat. During the measurement, an excitation source of He-Cd laser with laser line of 325 nm was used.

3 Results and discussion

To discuss the morphologies of the ZnO/ZnS core-shell heterostructured NWs after thermal treatments, scanning electron microscopy (SEM) images are shown in Figure 1a–d. Compared with the core-only ZnO NWs (in the supporting information Figure S1), the surface of the

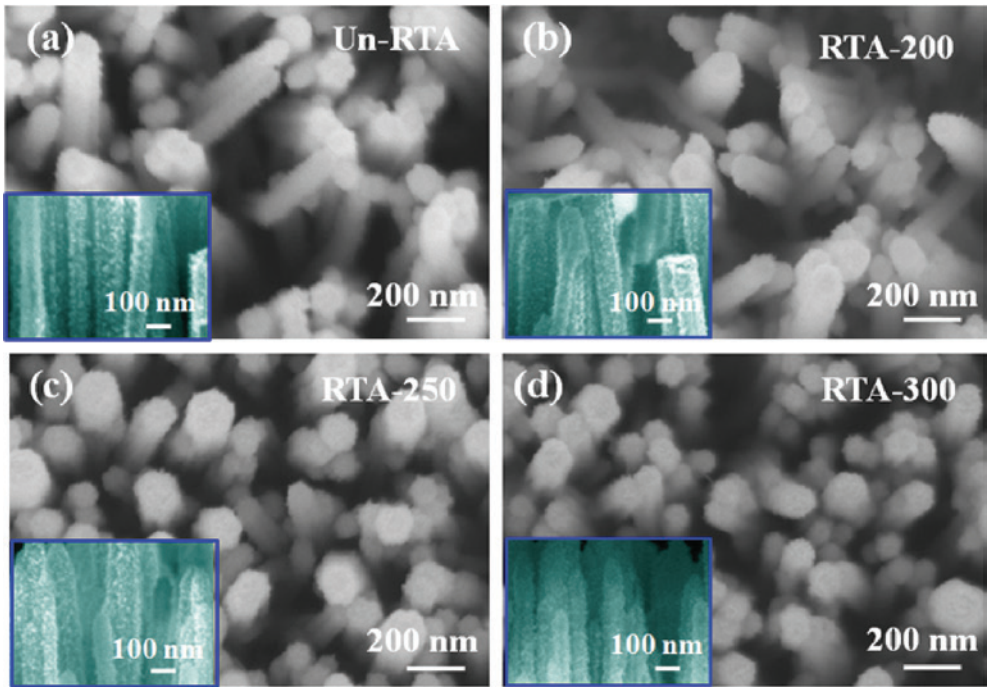

Figure 1: SEM images of ZnO/ZnS core-shell heterostructured NWs, the annealed 200°C (RTA-200), the annealed 250°C (RTA-250), and the annealed 300°C (RTA-300) NW samples. Insets show the individual NWs of samples' SEM images.

ZnO/ZnS NWs becomes rough, indicating the successful growth of ZnS shell structure. We can see from the sectional views that the surface roughness of the samples gradually decreases. A more clear description of the morphologies of the samples on the rapid thermal annealing (RTA) will be discussed below.

XRD measurements were performed to investigate the annealing-induced change of crystalline structures.

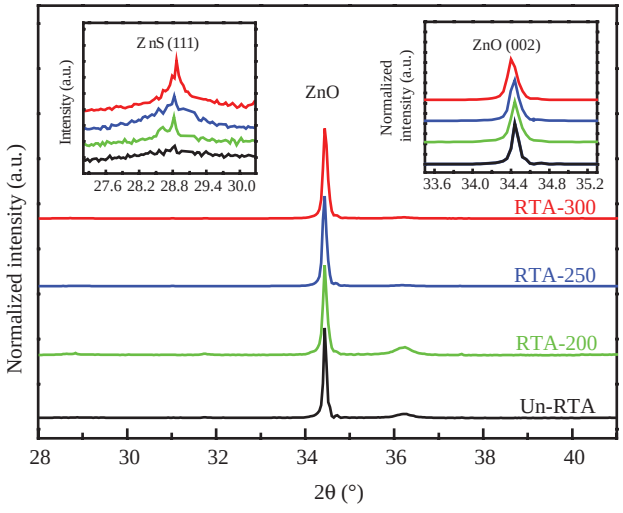

Figure 2: X-ray diffraction patterns of Un-RTA, RTA-200, RTA-250, and RTA-300, respectively.

Figure 2 shows the XRD patterns of the samples before and after annealing. We can observe that the peak at 34.44° and 28.83° can be identified to be the ZnO (002) and ZnS (111) of the core-shell NWs [25–27]. Among them, the peak intensity of ZnS (111) is weak along with a strong peak intensity of ZnO (002), indicating that the as-grown ZnO/ZnS core-shell heterostructured NWs have a better crystal quality for the ZnO core. The inset of Figure 2 clearly shows the annealing-induced evolution of the ZnS (111) and ZnO (002) diffraction peak. With the increase of annealing temperature, the diffraction peak intensity of ZnS (111) became stronger, implying that the crystal quality of ZnS shells have been improved after the annealing treatments. In addition, it is important to note that the (002) peak position of ZnO slightly blueshifts, while the peak position of ZnS (111) slightly redshifts for the sample RTA-300 as shown in Figure 2. The peak position shifting can be ascribed to formation of the ZnOS ternary alloy at the ZnO/ZnS NWs interface [26, 27]. Other supporting information for this claim will be provided and discussed later.

To investigate the influence of thermal treatments on the optical properties of the ZnO/ZnS core-shell heterostructured NWs, room temperature photoluminescence (RTPL) measurements were performed. As shown in Figure 3, the peak position of UV emission from Un-RTA ZnO/ZnS NWs is located at 3.284 eV, which is ascribed to the NBE emission from ZnO, and the peak position

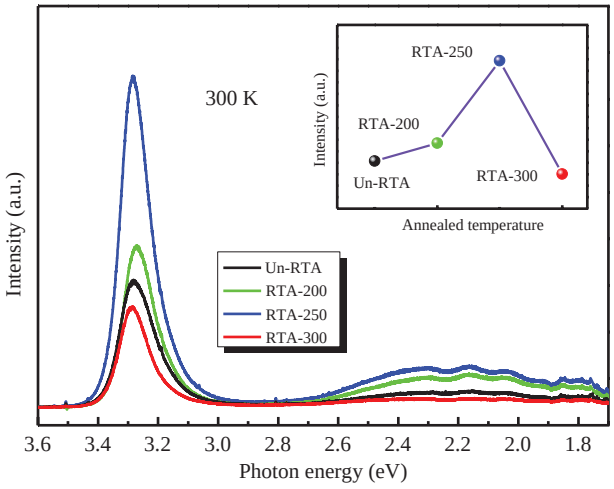

Figure 3: Room temperature PL spectra of Un-RTA, RTA-200, RTA-250, and RTA-300 samples. The inset is the peak intensity of the UV emission for different samples.

centered at approximately 2.2 eV is from the DLE [6, 20, 28]. Comparing with the Un-RTA sample, the UV peak positions of the RTA samples slightly change, while the UV and DLE intensity increase firstly and then decrease. As will be discussed later, the slight shifting of the UV emissions is due to the change of exciton-phonon coupling strength in the samples. According to the XRD results, the crystalline quality of ZnO/ZnS NWs is improved after annealing, and the RTA-300 sample shows the best crystalline quality. Generally speaking, semiconductor samples with a better crystalline quality can give rise to a stronger UV emission and a weaker DLE. However, from Figure 3, the RTA-250 has the strongest emission intensity of PL, and the RTA-300 has the weakest one in both UV emission and DLE. These abnormal trends are not consistent with the general rules of thermal treatments, and therefore, there must be other physical mechanisms caused by annealing. Compared with previous reports [6], the main reason for this abnormal trend is most likely the localized states at the ZnO/ZnS interface.

It is reported that the localized states can prevent excitons from diffusing to non-radioactive recombination centers and thus enhancing the light emission efficiency. Therefore, the abnormal trend of the PL from the ZnO/ZnS NWs after thermal treatments can be ascribed to the presence of localized states near the ZnO and ZnS interface. To understand the annealing-induced structural transformation at the interfaces, detailed TEM and high-resolution TEM (HRTEM) experiments have been carried out. As shown in Figure 4A, compared to the smooth surface of ZnO core (the inset), the Un-RTA ZnO/ZnS NWs have a clear rough surface after coating the ZnS layer. The surface roughness of RTA-200, RTA-250, and RTA-300 become smoother with the increase of annealing temperatures, which are consistent with the SEM results. In the HRTEM image of Un-RTA (Figure 4B), there is a clearer jagged boundary (the yellow solid line) at the interface between the ZnO core and ZnS shell. This boundary still clearly exists after thermal treatment at 200 and 250°C (supporting information Figure S2). However, with the increase of annealing temperature up to 300°C, the boundary of ZnO/ZnS NWs disappears (Figure 4C and D). The disappearing of jagged boundary was ascribed to the inter-diffusing of oxygen and sulfur atoms that lead to the formation of ZnOS ternary alloy, which is consistent with the XRD result. From the close-up region of corresponding areas (colored boxes) in Figure 4B, well-defined lattice fringes with planar *d*-spacing of 0.26 and 0.32 nm can be indexed as ZnO (002) plane (Figure 4E) and ZnS (111) plane (Figure 4F), demonstrating the successful construction of the core-shell heterostructure [28–30].

The evolution of the ZnO and ZnS atoms at the interface after the thermal treatments is important to confirm the formation of ZnOS. For this purpose, the close-up TEM image of the corresponding region at the interface of Un-RTA and RTA-300 samples were shown in Figure 4G and H. The ZnO and ZnS atoms are marked with different colors, and it is used to visually analyze the interface arrangement of two kinds of atoms. From Figure 4G, the ZnO and ZnS atoms at the interface can be clearly seen to form staggered arrangements with some atom clusters. This atom cluster may be the cause of localized states and is ascribed to their different lattice fringes with planar *d*-spacings. After the ZnO/ZnS NWs annealed in 300°C, as shown in Figure 4H, the staggered arrangements of ZnO and ZnS atom disappeared and gradually became orderly ones. The decrease of interfacial composition fluctuations and an inter-diffusion of oxygen and sulfur atoms resulted in a formation of ZnOS phase near the interface. These transformations can give rise to phenomena of the abnormal trend, which have already been described in the RTPL measurement.

To further investigate the influence of thermal treatments on the emission of localized excitons at the ZnO/ZnS NWs interface, TDPL measurement was carried out (supporting information Figure S3). The changes of peak positions and the FWHM of the TDPL spectra for ZnO/ZnS NWs with temperature were plotted, as shown in Figure 5. The "S-shape" feature of the peak position for the Un-RTA is more significant than the RTA samples. Moreover, it is worthy to note that the RTA-300 exhibits a totally different trend compared with other samples (Figure 5A). As shown

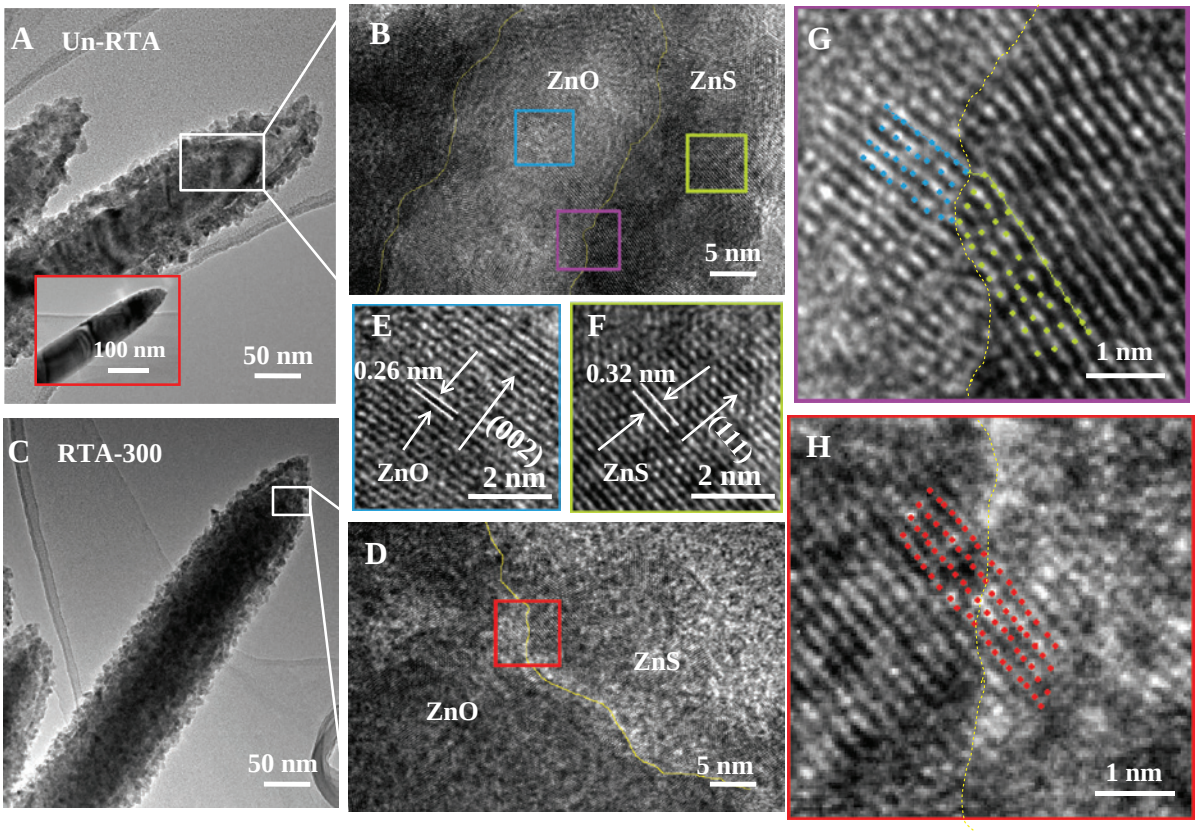

Figure 4: TEM images of individual NWs of (A) Un-RTA (the inset is the ZnO NWs) and (C) the RTA-300; (B) and (D) show the corresponding HRTEM images. The solid line in the HRTEM image in (B) and (D) marks the ZnO/ZnS NWs interface. The left half of the ZnO core is marked out with a blue square, and the right half of the ZnS shell is marked out with a green square; (E) and (F) are the enlarged phase images of the ZnO core and the ZnS shell from the marked area of image (B). (G) and (H) Close-up HRTEM images of the interface between the ZnO core and the ZnS shell, showing the stacking grain boundaries and fluctuations of atoms in space as well as the ZnOS phase at the interface area.

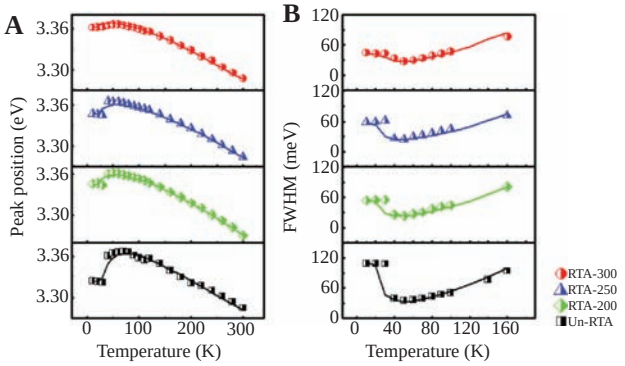

Figure 5: (A) Temperature-dependent peak position of the ZnO/ZnS NWs before and after annealing. (B) The FWHM parameter of the ZnO/ZnS NWs before and after annealing vs. temperature. The solid lines represent theoretical curve according to the proposed luminescence model of the LSE.

in Figure 5B, the curves of FWHM show the "valley-shape" features that gradually disappear after thermal treatments. The "S-shape" and "valley-shape" characteristics obtained from the samples' emission have further confirmed the existence of localized states, which is consistent with previous reports [1, 2, 6–8].

The model for the luminescence of localized-state ensemble (LSE), which can be used to depict the thermal redistribution of localized carriers within the localized states, is used to analyze the behavior of localized excitonic emission at different temperatures [5]. According to the model, the temperature-dependent emission peak is given by

$$E(T) = E_0 - \frac{\alpha T^2}{\beta + T} - x \cdot k_B T \quad (1)$$

The first two terms of the formula describe the traditional bandgap shrinking. The value of α is the Varshni parameter, and β is the Debye temperature, which are material dependent. The third term of the formula is an environment-dependent parameter and represents the effect of thermal redistribution of localized carriers. The value of k_B is the Boltzman constant, and

Table 1: The fitting parameters obtained from LSE luminescence model for the four samples.

ZnO/ZnS NWs	E_0[a] (eV)	$E_0 - E_a$[b] (meV)	τ_{tr}/τ_r[c] (ps/ps)	σ[a] (meV)	α[d] (meV/K)	β[d] (K)
Un-RTA	3.37872	40.37	0.00208/293.1	11.1	0.636	300
RTA-200	3.37337	16.77	0.00387/369.4	7.1	0.671	300
RTA-250	3.37610	14.54	0.00484/381.7	6.3	0.666	300
RTA-300	3.37830	7.58	0.027593/438.4	5.2	0.662	356

[a]E_0 and σ are the central energy and broadening parameter for the distribution of the localized states, respectively; [b]$E_0 - E_a$ is in effect the thermal activation energy of the carriers; [c]τ_{tr} is the ratio of the escape time constant, and τ_r is the radiative recombination time constant; this value is considered by Ref. [31]; [d]α is the Varshni parameter, and β is the Debye temperature; this value is considered by Ref. [32].

the dimensionnless coefficient $x(T)$ can be obtained by numerically solving the following equation [5]:

$$xe^x = \left[\left(\frac{\sigma}{k_B T}\right)^2 - x\right]\left(\frac{\tau_r}{\tau_{tr}}\right)e^{(E_0 - E_a)/k_B T} \quad (2)$$

where E_0 and σ are the peak energy position and the standard deviation of distribution of the DOS, respectively. The term $1/\tau_{tr}$ is the escape rate, and $1/\tau_r$ is the radiative recombination rate of the localized carriers. It is noted that the value of $E_0 - E_a$ is one of the most important parameters for the system and representes the degree of the localization. For the case of $E_0 > E_a$, the luminescence peak positions show the typical "S-shape" characteristics. The larger the absolute value of $E_0 - E_a$, the deeper the localized states, and the less likely for the carriers to escape from the localized state.

At high temperatures, the solution of equation (2) can be found to be $x \approx (\sigma/k_B T)^2$ and equation (1) becomes

$$E(T) = E_0 - \frac{\alpha T^2}{\beta + T} - \frac{\sigma^2}{k_B T}. \quad (3)$$

which can be used to estimate the value of σ.

FWHM height is another parameter for a luminescence spectrum, which is embedded in the localized excitons distribution function of $n(E, T)$:

$$n(E,T) = \frac{\rho_0 e^{-(E-E_0)^2/2\sigma^2}}{e^{(E-E_a)k_B T} + \tau_{tr}/\tau_r} \quad (4)$$

where $\rho(E) = \rho_0 e^{-(E-E_0)^2/2\sigma^2}$ represents the LSE system with a Gaussian-type DOS. ρ_0 is the amplitude of DOS in $T = 0$ K, which is a material-dependent constant and is independent of the half-line-width value. The FWHM of $n(E, T)$ can be obtained by numerically solving the following equations.

$$n(E_{2,1}, T) = n(E_{pk}, T)/2 \quad (5)$$

$$\text{FWHM} = E_2 - E_1 \quad (6)$$

where E_{pk} is the peak position. As shown in Figure 5, the variation of FWHM with temperature exhibits a "valley shape".

As can be seen in Figure 5A and B, the solid lines are the curves obtained from the LSE model for Un-RTA and RTA-samples, respectively. The above results confirm the existence of localized states at the ZnO/ZnS NWs. The fitted parameters obtained from LSE luminescence model for the four samples are shown in Table 1. It is noted that the fitted $E_0 - E_a$ value decrease from 40.37 to 7.58 meV for the Un-RTA to the RTA-300 samples, which indicates that the localized degree gradually reduces after thermal treatments. Besides, according to the reduced localized degree, both the radiative recombination rate of the localized carriers $1/\tau_r$ and the escape rate of $1/\tau_{tr}$ decrease, which implies that the carriers can more likely escape from the localized traps. The broadening parameter σ is essentially related to the distribution width of the localized states, which is closely related to the localized degree in the material system. It is noted that a bigger localized degree will lead to a wider distribution width of the localized states, so the values of σ are getting smaller after the thermal treatments. Moreover, the RTA-300 sample has different values of β compared with other ones, indicating that a new phase of ZnOS is formed at the ZnO/ZnS interface. Therefore, the above phenomena imply that the thermal treatment is one of the effective ways to reduce the localized degree.

4 Conclusions

In conclusion, the localized states were introduced at the ZnO/ZnS NWs through the core-shell structure constructed via the wet chemical method. The morphological, structural, and optical properties of the ZnO/ZnS core-shell heterostructured NWs are sensitive to the thermal treatments. It was found that the staggered arrangement of ZnO and ZnS atoms at the interface of ZnO/ZnS NWs

gradually became ordered ones, and the roughness of surface becomes smoother with the increase of thermal treatment temperatures. The characteristics of the "S shape" and "valley shape" gradually disappeared after thermal treatments, indicating that most of the localized excitons are de-trapped and show delocalized excitonic emission. Therefore, the thermal treatment is an effective way to manipulate the localized states at the ZnO/ZnS NWs interface and is very important for their potential device applications.

Acknowledgments: This work is supported by the National Natural Science Foundation of China (61307045, 61404009, 61474010, 61574022, 61504012, 11404219, 11404161, and 11574130), the Foundation of State Key Laboratory of High Power Semiconductor Lasers, the Developing Project of Science and Technology of Jilin Province (20160519007JH and 20160520117JH), and the Project of Education Department of Jilin Province [2015(70)]. R. C. acknowledges the support from National 1000 Plan for young talents and Shenzhen Science and Technology Innovation Committee (Projects Nos. JCYJ20150630162649956, JCYJ20150930160634263, and KQTD2015071710313656).

References

1. Erol A. Materials Science, Springer: New York, NY, USA 2008; Chapter 7, pp. 181–194.
2. He H, Yu Q, Li H, et al. Exciton localization in solution-processed organolead trihalide perovskites. Nat Commun 2016;7: 10896–906.
3. Tighineanu PR, Daveau E, Lee H, et al. Decay dynamics and exciton localization in large GaAs quantum dots grown by droplet epitaxy. Phys Rev B 2013;88:155320.
4. Zhu H, Shan CX, Li BH, et al. Enhanced photoluminescence caused by localized excitons observed in MgZnO alloy. J Appl Phys 2009;105:103508.
5. Li Q, Xu SJ, Xie MH, Tong SY. A model for steady-state luminescence of localized-state ensemble. Europhys Lett 2005;71:994–1000.
6. Fang X, Wei Z, Yang Y, et al. Ultraviolet electroluminescence from ZnS@ZnO core-shell nanowires/p-GaN introduced by exciton localization. ACS Appl Mater Interf 2016;8:1661–6.
7. Chen R, Ye QL, He T, et al. Exciton localization and optical properties improvement in nanocrystal-embedded ZnO core-shell nanowires. Nano Lett 2013;13:734–9.
8. Fang X, Wei Z, Chen R, et al. Influence of exciton localization on the emission and ultraviolet photoresponse of ZnO/ZnS core-shell nanowires. ACS Appl Mater Interf 2015;7:10331–6.
9. Kohno T, Sudo Y, Yamauchi M, et al. Internal quantum efficiency and nonradiative recombination rate in InGaN-based near-ultraviolet light-emitting diodes. Jpn J Appl Phys 2012;51:072102.
10. Monemar B, Sernelius BE. Defect related issues in the "current roll-off" in InGaN based light emitting diodes. Appl Phys Lett 2007;91:181103.
11. Chichibu SF, Uedono A, Onuma T, et al. Origin of defect-insensitive emission probability in In-containing (Al, In, Ga) N alloy semiconductors. Nat Mater 2006;5:810–6.
12. Gregg BA. Excitonic solar cells. J Phys Chem B 2003;107:4688–98.
13. Pradel KC, Ding Y, Wu W, Bando Y, Fukata N, Wang ZL. Optoelectronic properties of solution grown ZnO np or pn core-shell nanowire arrays. ACS Appl Mater Interf 2016:8:4287–91.
14. Guo Z, Li H, Zhou L, et al. Large-scale horizontally aligned ZnO microrod arrays with controlled orientation, periodic distribution as building blocks for chip-in piezo-phototronic LEDs. Small 2015;11:438–45.
15. Nasiri N, Bo R, Wang F, Fu L, Tricoli A. Ultraporous electron-depleted ZnO nanoparticle networks for highly sensitive portable visible-blind UV photodetectors. Adv Mater 2015;27:4336–43.
16. Dang VQ, Trung TQ, Kim D, et al. Ultrahigh responsivity in graphene-ZnO nanorod hybrid UV photodetector. Small 2015;11:3054–65.
17. Liu X, Gu L, Zhang Q, Wu J, Long Y, Fan Z. All-printable band-edge modulated ZnO nanowire photodetectors with ultra-high detectivity. Nat Commun 2014;5:4007–16.
18. Guo F, Yang B, Yuan Y, et al. A nanocomposite ultraviolet photodetector based on interfacial trap-controlled charge injection. Nat Nanotechnol 2012;7:798–802.
19. Soci C, Zhang A, Xiang B, et al. ZnO nanowire UV photodetectors with high internal gain. Nano Lett 2007;7:1003–9.
20. Hsu CL, Chang SJ. Doped ZnO 1D nanostructures: synthesis, properties, and photodetector application. Small 2014;10:4562–85.
21. Tian W, Zhang C, Zhai T, et al. Flexible ultraviolet photodetectors with broad photoresponse based on branched ZnS-ZnO heterostructure nanofilms. Adv Mater 2014;26:3088–93.
22. Tian ZR, Voigt JA, Liu J, et al. Complex and oriented ZnO nanostructures. Nat Mater 2003;2:821–6.
23. Sun M, Xu Z, Yin M, et al. Broad-band three dimensional nanocave ZnO thin film photodetectors enhanced by Au surface plasmon resonance. Nanoscale 2016;8:8924–30.
24. Liu KW, Chen R, Xing GZ, Wu T, Sun HD. Photoluminescence characteristics of high quality ZnO nanowires and its enhancement by polymer covering. Appl Phys Lett 2010;96:023111.
25. Jeong S, Choe M, Kang JW, et al. High-performance photoconductivity and electrical transport of ZnO/ZnS core/shell nanowires for multifunctional nanodevice applications. ACS Appl Mater Interf 2014;6:6170–6.
26. Meyer BK, Polity A, Farangis B, et al. Structural properties and bandgap bowing of $ZnO_{1-x}S_x$ thin films deposited by reactive sputtering. Appl Phys Lett 2004;85:4929–31.
27. Baldissera G, Persson C. Understanding the optical properties of $ZnO_{1-x}S_x$ and $ZnO_{1-x}Se_x$ alloys. J Appl Phys 2016;119:045704.
28. Bera A, Basak D. Photoluminescence and photoconductivity of ZnS-coated ZnO nanowires. ACS Appl Mater Interf 2010;2:408–12.
29. Hu H, Wang K, Long H, Liu W, Wang B, Lu P. Precise determination of the crystallographic orientations in single ZnS

nanowires by second-harmonic generation microscopy. Nano Lett 2015;15:3351–7.
30. Chen R, Li D, Liu B, et al. Optical and excitonic properties of crystalline ZnS nanowires: toward efficient ultraviolet emission at room temperature. Nano Lett 2010;10:4956–61.
31. Ren QJ, Filippov S, Chen SL, et al. Evidence for coupling between exciton emissions and surface plasmon in Ni-coated ZnO nanowires. Nanotechnology 2012;23:425201.
32. Chen R, Ye QL, He TC, Wu T, Sun DH. Uniaxial tensile strain and exciton-phonon coupling in bent ZnO nanowires. Appl Phys Lett 2011;98:241916.

Supplemental Material: The online version of this article (DOI: 10.1515/nanoph-2016-0157) offers supplementary material, available to authorized users.